

Uncertainty Quantification and Deep Ensembles

Rahul Rahaman^{*} and Alexandre H. Thiery[†]

Department of Statistics,
National University of Singapore

March 23, 2022

Abstract

Deep Learning methods are known to suffer from calibration issues: they typically produce over-confident estimates. These problems are exacerbated in the low data regime. Although the calibration of probabilistic models is well studied, calibrating extremely over-parametrized models in the low-data regime presents unique challenges. We show that deep-ensembles do not necessarily lead to improved calibration properties. In fact, we show that standard ensembling methods, when used in conjunction with modern techniques such as mixup regularization, can lead to less calibrated models. In this text, we examine the interplay between three of the most simple and commonly used approaches to leverage deep learning when data is scarce: data-augmentation, ensembling, and post-processing calibration methods. We demonstrate that, although standard ensembling techniques certainly help to boost accuracy, the calibration of deep-ensembles relies on subtle trade-offs. Our main finding is that calibration methods such as temperature scaling need to be slightly tweaked when used with deep-ensembles and, crucially, need to be executed *after* the averaging process. Our simulations indicate that, in the low data regime, this simple strategy can halve the Expected Calibration Error (ECE) on a range of benchmark classification problems when compared to standard deep-ensembles.

1 Introduction

Overparametrized deep models can memorize datasets with labels entirely randomized [ZBH⁺16]. It is consequently not entirely clear why such extremely flexible models are able to generalize well on unseen data and trained with algorithms as simple as stochastic gradient descent, although a lot of progress on these questions have recently been reported [DR17, JGH18, BM19, MMN18, RVE18, GML⁺18].

^{*}rahul.rahaman@u.nus.edu

[†]a.h.thiery@nus.edu.sg

The high-capacity of neural network models, and their ability to easily overfit complex datasets, makes them especially vulnerable to calibration issues. In many situations, standard deep-learning approaches are known to produce probabilistic forecasts that are over-confident [GPSW17]. In this text, we consider the regime where the size of the training sets are very small, which typically amplifies these issues. This can lead to problematic behaviours when deep neural networks are deployed in scenarios where a proper quantification of the uncertainty is necessary. Indeed, a host of methods [LPB17, MGI⁺19, SHK⁺14, GG16, Pre98] have been proposed to mitigate these calibration issues, even though no gold-standard has so far emerged. Many different forms of regularization techniques [PW17, ZBH⁺16, ZH05] have been shown to reduce overfitting in deep neural networks. Importantly, practical implementations and approximations of Bayesian methodologies [MGI⁺19, WHSX16, BCKW15, Gra11, LW16, RMW14, Mac92] have demonstrated their worth in several settings, although some of these techniques are not entirely straightforward to implement in practice. Ensembling approaches such as *drop-outs* [GG16] have been widely adopted, largely due to their ease of implementation. In this text, we investigate the practical use of Deep-Ensembles [LPB17, BC17, LPC⁺15, SLJ⁺15, FHL19, GPSW17], a straightforward approach that displays state-of-the-art performances in most regimes. Although deep-ensembles can be difficult to implement when training datasets are large (but calibration issues are less pronounced in this regime), the focus of this text is the data-scarce regime where the computational burden associated to deep-ensembles is not a significant problem.

Contributions: we study the interaction between three of the most simple and widely used methods for scaling deep-learning to the low-data regime: ensembling, temperature scaling, and mixup data-augmentation.

- Despite the general belief that averaging models improves calibration properties, we show that, in general, standard ensembling practices do not lead to better-calibrated models. Instead, we show that averaging the predictions of a set of neural networks generally leads to less confident predictions: that is generally only beneficial in the oft-encountered regime when each network is overconfident. Although our results are based on Deep Ensembles, our empirical analysis extends to any class of model averaging, including sampling-based Bayesian Deep Learning.
- We empirically demonstrate that networks trained with the *mixup* data-augmentation scheme, a very common practice in computer vision, are typically under-confident. Consequently, subtle interactions between ensembling techniques and modern data-augmentation pipelines have to be taken into account for proper uncertainty quantification. The typical distributional-shift induced by the mixup data-augmentation strategy influences the calibration properties of the resulting trained neural networks.
- Post-processing techniques such as *temperature scaling* can be successfully used in conjunction with deep-ensembling methods, but the order in which the aggregation and the calibration procedures are carried out does greatly influence the quality of the resulting uncertainty quantification. These findings lead us to formulate the straightforward *Pool-Then-Calibrate* strategy for post-processing deep-ensembles: (1) in a first stage, separately

train deep models (2) in a second stage, fit a *single* temperature parameter by minimizing a proper scoring rule (eg. cross-entropy) on a validation set. In the low data-regime, this simple procedure can halve the Expected Calibration Error (ECE) on a range of benchmark classification problems when compared to standard deep-ensembles.

2 Background

Consider a classification task with $C \geq 2$ possible classes $\mathcal{Y} \equiv \{1, \dots, C\}$. For a sample $x \in \mathcal{X}$, the quantity $\mathbf{p}(x) \in \Delta_C = \{\mathbf{p} \in \mathbb{R}_+^C : p_1 + \dots + p_C = 1\}$ represents a probabilistic prediction, often obtained as $\mathbf{p}(x) = \sigma_{\text{SM}}[\mathbf{f}_w(x)]$ for a neural network $\mathbf{f}_w : \mathcal{X} \rightarrow \mathbb{R}^C$ with weight $w \in \mathbb{R}^D$ and softmax function $\sigma_{\text{SM}} : \mathbb{R}^C \rightarrow \Delta_C$. We set $\hat{y}(x) \equiv \arg \max \mathbf{p}(x)$ and $\hat{p}(x) = \max \mathbf{p}(x)$.

Augmentation: Consider a training dataset $\mathcal{D} \equiv \{x_i, y_i\}_{i=1}^N$ and denote by $\bar{y} \in \Delta_C$ the one-hot encoded version of the label $y \in \mathcal{Y}$. A stochastic augmentation process $\text{Aug} : \mathcal{X} \times \Delta_C \rightarrow \mathcal{X} \times \Delta_C$ maps a pair $(x, \bar{y}) \in \mathcal{X} \times \Delta_C$ to another augmented pair (x_*, \bar{y}_*) . In computer vision, standard augmentation strategies include rotations, translations, brightness and contrast manipulations. In this text, in addition to these standard agumentations, we also make use of the more recently proposed *mixup* augmentation strategy [ZCDL17] that has proven beneficial in several settings. For a pair $(x, \bar{y}) \in \mathcal{X} \times \Delta_C$, its mixup-augmented version (x_*, \bar{y}_*) is defined as

$$x_* = \gamma x + (1 - \gamma) x_J \quad \text{and} \quad \bar{y}_* = \gamma \bar{y} + (1 - \gamma) \bar{y}_J \quad (1)$$

for a random coefficient $\gamma \in (0, 1)$ drawn from a fixed mixing distribution often chosen as $\text{Beta}(\alpha, \alpha)$, and a random index J drawn uniformly within $\{1, \dots, N\}$.

Model averaging: Ensembling methods leverage a set of models by combining them into a aggregated model. In the context of deep learning, Bayesian averaging consists in weighting the predictions according to the Bayesian posterior $\pi(dw \mid \mathcal{D}_{\text{train}})$ on the neural weights. Instead of finding an optimal set of weights by minimizing a loss function, predictions are averaged. Denoting by $\mathbf{p}_w(x) \in \Delta_C$ the probabilistic prediction associated to sample $x \in \mathcal{X}$ and neural weight w , the Bayesian approach advocates to consider

$$(\text{prediction}) \equiv \int \mathbf{p}_w(x) \pi(dw \mid \mathcal{D}_{\text{train}}) \in \Delta_C. \quad (2)$$

Designing sensible prior distributions is still an active area of research and data-augmentation schemes, crucial in practice, are not entirely straightforward to fit into this framework. Furthermore, the high-dimensional integral (2) is (extremely) intractable: the posterior distribution $\pi(dw \mid \mathcal{D}_{\text{train}})$ is multi-modal, high-dimensional, concentrated along low-dimensional structures, and any local exploration algorithm (eg. MCMC, Langevin dynamics and their variations) is bound to only explore a tiny fraction of the state space. Because of the typically large number of degrees of symmetries, many of these local modes correspond to essentially similar predictions, indicating that it is likely not necessary to explore all the modes in order to approximate (2). A detailed understanding of the geometric properties of the posterior distribution in Bayesian neural

networks is still lacking, although a lot of recent progress have been made. Indeed, variational approximations have been reported to improve, in some settings, over standard empirical risk minimization procedures. Deep-ensembles can be understood as crude, but practical, approximations of the integral in Equation (2). The high-dimensional integral can be approximated by a simple non-weighted average over several modes $\mathbf{w}_1, \dots, \mathbf{w}_K$ of the posterior distribution found by minimizing the negative log-posterior, or some approximations of it, with standard optimization techniques:

$$(\text{prediction}) \equiv \frac{1}{K} \left\{ \mathbf{p}_{\mathbf{w}_1}(x) + \dots + \mathbf{p}_{\mathbf{w}_K}(x) \right\} \in \Delta_C. \quad (3)$$

We refer the interested reader to [Nea12, MMK03, WI20] for different perspectives on Bayesian neural network. Although simple and not very well understood, deep-ensembles have been shown to provide extremely robust uncertainty quantification when compared to more sophisticated approaches [LPB17, BC17, LPC⁺15, SLJ⁺15].

Post-processing Calibration Methods: The article [GPSW17] proposes a class of post-processing calibration methods that extend the more standard *Platt Scaling* approach [Pla99]. *Temperature Scaling*, the simplest of these methods, transforms the probabilistic outputs $\mathbf{p}(x) \in \Delta_C$ into a tempered version $\text{Scale}[\mathbf{p}(x), \tau] \in \Delta_C$ defined through the scaling function

$$\text{Scale}(\mathbf{p}, \tau) \equiv \sigma_{\text{SM}}(\log \mathbf{p}/\tau), \quad (4)$$

for a temperature parameter $\tau > 0$. The optimal parameter $\tau_* > 0$ is usually found by minimizing a proper-scoring rules [GR07], often chosen as the negative log-likelihood, on a validation dataset. Crucially, during this post-processing step, the parameters of the probabilistic model are kept fixed: the only parameter being optimized is the temperature $\tau > 0$. In the low-data regime considered in this article, the validation set being also extremely small, we have empirically observed that the more sophisticated *Vector* and *Matrix* scaling post-processing calibration methods [GPSW17] do not offer any significant advantage over the simple and robust temperature scaling approach.

Calibration Metrics: The *Expected Calibration Error* (ECE) measures the discrepancy between prediction confidence and empirical accuracy. In this text, we also define the *signed Expected Calibration Error* (sECE) in order to differentiate under-confidence from over-confidence. For a partition $0 = c_0 < \dots < c_M = 1$ of the unit interval and a labelled set $\{x_i, y_i\}_{i=1}^N$, set $B_m = \{i : c_{m-1} < \hat{p}(x_i) \leq c_m\}$ and $\text{acc}_m = \frac{1}{|B_m|} \sum_{i \in B_m} \mathbf{1}(\hat{y}(x_i) = y_i)$ and $\text{conf}_m = \frac{1}{|B_m|} \sum_{i \in B_m} \hat{p}(x_i)$. The quantities ECE and sECE are defined as

$$\text{ECE} = \sum_{m=1}^M \frac{|B_m|}{N} \left| \text{conf}_m - \text{acc}_m \right| \quad \text{and} \quad \text{sECE} = \sum_{m=1}^M \frac{|B_m|}{N} \left(\text{conf}_m - \text{acc}_m \right). \quad (5)$$

A model is calibrated if $\text{acc}_m \approx \text{conf}_m$ for all $1 \leq m \leq M$, i.e. $\text{ECE} \approx 0$. A large (resp. low) value of the sECE indicates over-confidence (resp. under-confidence). It is often instructive to display the associated *reliability curve*, i.e. the curve with conf_m on the x-axis and the difference

$(\text{acc}_m - \text{conf}_m)$ on the y-axis. Figure 1 displays examples of such reliability curves. A perfectly calibrated model is flat (i.e. $\text{acc}_m - \text{conf}_m = 0$), while the reliability curve associated to an under-confident (resp. over-confident) model prominently lies above (resp. below) the flat line $\text{acc}_m - \text{conf}_m = 0$. In the sequel, we sometimes report the value of the Brier score [Bri50] defined as $\frac{1}{N} \sum_{i=1}^N \|\mathbf{p}(x_i) - \bar{y}_i\|_2^2$.

3 Empirical Observations

Linear pooling: It has been observed in several studies that averaging the probabilistic predictions of a set of independently trained neural networks, i.e. deep-ensembles, often leads to more accurate and better-calibrated forecasts [LPB17, BC17, LPC⁺15, SLJ⁺15, FHL19]. Figure 1 displays the reliability curves across three different datasets of a set of $K = 30$ independently trained neural networks, as well as the reliability curves of the aggregated forecasts obtained by simply linear averaging the $K = 30$ individual probabilistic predictions. These results suggest that deep-ensembles consistently lead to predictions that are *less confident* than the ones of its individual constituents. This can indeed be beneficial in the often encountered situation when each individual neural network is overconfident. Nevertheless, this phenomenon should not be mistaken with an intrinsic property of deep ensembles to lead to better-calibrated forecasts. For example, and as discussed further in Section 4, networks trained with the popular *mixup* data-augmentation are typically under-confident. Ensembling such a set of individual networks typically leads to predictions that are even more under-confident. In order to gain some insights into this phenomenon, recall the definition of the entropy functional $\mathcal{H} : \Delta_C \rightarrow \mathbb{R}$,

$$\mathcal{H}(\mathbf{p}) = - \sum_{k=1}^C p_k \log p_k. \quad (6)$$

The entropy functional is concave on the probability simplex Δ_C , i.e. $\mathcal{H}(\lambda \mathbf{p} + (1 - \lambda) \mathbf{q}) \geq \lambda \mathcal{H}(\mathbf{p}) + (1 - \lambda) \mathcal{H}(\mathbf{q})$ for any $\mathbf{p}, \mathbf{q} \in \Delta_C$. Furthermore, tempering a probability distribution \mathbf{p} leads to increase in entropy if $\tau > 1$, as can be proved by examining the derivative of the function $\tau \mapsto \mathcal{H}[\mathbf{p}^{1/\tau}]$. The entropy functional is consequently a natural surrogate measure of (lack of) confidence. The concavity property of the entropy functional shows that ensembling a set of K individual networks leads to predictions whose entropies are higher than the average of the entropies of the individual predictions. We have not been able to prove a similar property for the ECE functional.

In order to obtain a more quantitative understanding of this phenomenon, consider a binary classification framework. For a pair of random variables (X, Y) , with $X \in \mathcal{X}$ and $Y \in \{-1, 1\}$, and a classification rule $p : \mathcal{X} \rightarrow [0, 1]$ that approximates the conditional probability $p_x \approx \mathbb{P}(Y = 1 | X = x)$, define the *Deviation from Calibration* score as

$$\text{DC}(p) \equiv \mathbb{E} \left[(\mathbf{1}_{\{Y=1\}} - p_X)^2 - p_X(1 - p_X) \right]. \quad (7)$$

The term $\mathbb{E} \left[(\mathbf{1}_{\{Y=1\}} - p_X)^2 \right]$ is equivalent to the Brier score of the classification rule p and the quantity $\mathbb{E}[p_X(1 - p_X)]$ is an entropic term (i.e. large for predictions close to uniform). Note that

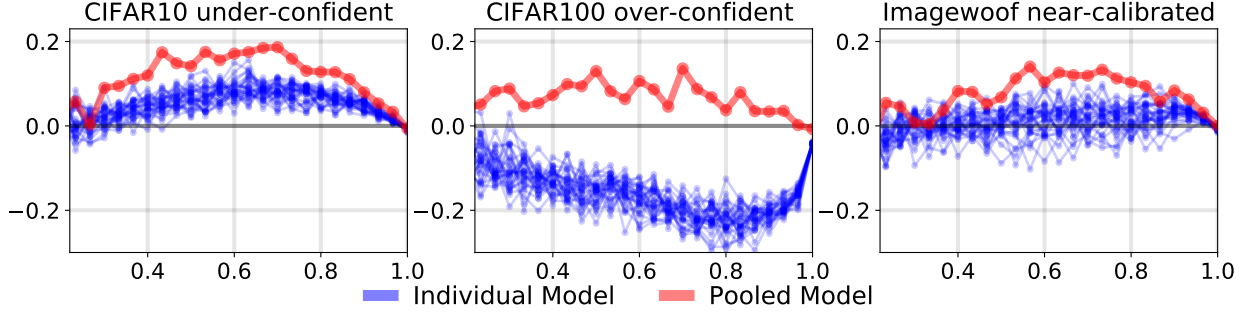


Figure 1: *Reliability Curves* with confidence conf_m on the x-axis and difference $(\text{acc}_m - \text{conf}_m)$ on the y-axis: see Section 2 for definitions. The plots display the reliability curves of $K = 30$ individual networks trained on three datasets (i.e. CIFAR10, CIFAR100 and IMAGEWOOF [How]), as well as the pooled estimates obtained by averaging the K individual predictions. This linear averaging leads to consistently less confident predictions (i.e. higher values of $(\text{acc}_m - \text{conf}_m)$). It is only beneficial to calibration when each network is over-confident. It is typically detrimental to calibration when the individual networks are already calibrated, or under-confident.

DC can take both positive and negative values and $\text{DC}(p) = 0$ for a well-calibrated classification rule, i.e. $p_x = \mathbb{P}(Y = 1|X = x)$ for all $x \in \mathcal{X}$. Furthermore, among a set of classification rules with the same Brier score, the ones with less confident predictions (i.e. larger entropy) have a lesser DC score. In summary, the DC score is a measure of confidence that vanishes for well-calibrated classification rules, and that is low (resp. high) for under-confident (resp. over-confident) classification rules. Contrarily to the entropy functional (6), the DC score is extremely tractable. Algebraic manipulations readily shows that, for a set of $K \geq 2$ classification rules $p^{(1)}, \dots, p^{(K)}$ and non-negative weights $\omega_1 + \dots + \omega_K = 1$, the linearly averaged classification rule $\sum_{i=1}^K \omega_i p^{(i)}$ satisfies

$$\text{DC}\left(\sum_{i=1}^K \omega_i p^{(i)}\right) = \sum_{i=1}^K \omega_i \text{DC}(p^{(i)}) - \underbrace{\sum_{i,j=1}^K \omega_i \omega_j \mathbb{E}\left[\left(p_X^{(i)} - p_X^{(j)}\right)^2\right]}_{\geq 0}. \quad (8)$$

Equation (8) shows that averaging classifications rules decreases the DC score (i.e. the aggregated estimates are less confident). Furthermore, the more dissimilar the individual classification rules, the larger the decrease. Even if each individual model is well-calibrated, i.e. $\text{DC}(p^{(i)}) = 0$ for $1 \leq i \leq K$, the averaged model is not well-calibrated as soon as at least two of them are not identical.

Distance to the training set: in order to gain some additional insights into the calibration properties of neural networks trained on small datasets, as well as the influence of the popular mixup augmentation strategy, we examine several metrics (i.e. signed ECE (sECE), Negative Log-likelihood (NLL), entropy) as a function of the distance to the (small) training set $\mathcal{D}_{\text{train}}$. We focus on the CIFAR10 dataset and train our networks on a balanced subset of $N = 1000$ training examples. Since there is no straightforward and semantically meaningful distance between images, we first use an unsupervised method (i.e. labels were not used) for learning a low-dimensional and semantically meaningful representation of dimension $d = 128$. For these experiments, we obtained a mapping $\Phi : \mathbb{R}^{32,32} \rightarrow \mathbb{S}^{128}$, where $\mathbb{S}^{128} \subset \mathbb{R}^{128}$ denotes the unit sphere in

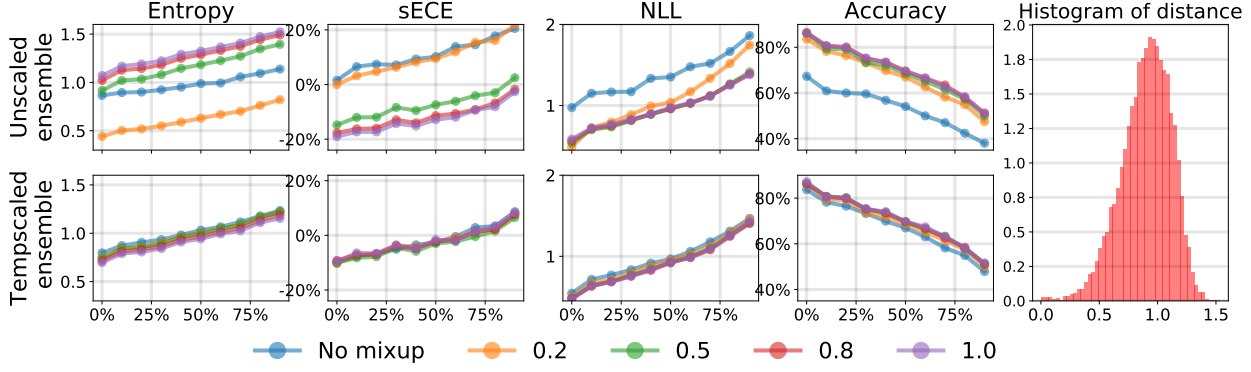


Figure 2: Deep Ensembles trained on $N = 1000$ CIFAR10 samples with different amount of mixup regularization. The x-axis represents a quantile of the distance to the CIFAR10 training set (see Section 3 for details). The overall distribution of the distances is displayed in the last column. The first row describes the performances of standard Deep Ensembles trained with data-augmentation and several amounts of mixup regularization. In the second row, before averaging the predictions of the members of the ensemble, each individual network is first temperature scaled on a validation set of size $N_{\text{val}} = 50$: this corresponds to method **(B)** of Section 4.

\mathbb{R}^{128} , with the *simCLR* method of [CKNH20], although experiments with other metric learning approaches [HFW⁺19, YZYC19] have led to essentially similar conclusions. We used the distance $d(x, y) = \|\Phi(x) - \Phi(y)\|_2$, which in this case is equivalent to the cosine distance between the 128-dimensional representations of the CIFAR10 images x and y . The distance of a test image x to the training dataset is defined as $\min\{d(x, y_i) : y_i \in \mathcal{D}_{\text{train}}\}$. We computed the distances to the training set for each image contained in the standard CIFAR10 test set (last column of Figure 2). Not surprisingly, we note that the average Entropy, Negative Log-likelihood and Error Rate all increase as test samples are chosen further away from the training set.

- **Over-confidence:** the predictions associated to samples chosen further away from the training set have a higher sECE. This indicates that the *over-confidence* of the predictions increases with the distance to the training set. In other words, even if the entropy increases as the distance increases (as it should), calibration issues do not vanish as the distance to the training set increases. This phenomenon is irrespective of the amount of mixup used for training the network.
- **Effect of mixup-augmentation:** The first row of Figure 2 shows that increasing the amount of mixup augmentation consistently leads to an increase in entropy, decrease in over-confidence (i.e. sECE), as well as a more accurate predictions (lower NLL and higher accuracy). Additionally, the effect is less pronounced for $\alpha \geq 0.2$. This is confirmed in Figure 3 that displays the more generally the effect of the mixup-augmentation on the reliability curves, over four different datasets.
- **Temperature Scaling:** importantly, the second row of Figure 2 indicates that a post-processing temperature scaling for the individual models almost washes-out all the differences due to the mixup-augmentation scheme. For this experiment, an ensemble of $K = 30$ networks is considered: before averaging the predictions, each network has been individu-

ally temperature scaled by fitting a temperature parameter (through negative likelihood minimization) on a validation set of size $N_{\text{valid}} = 50$.

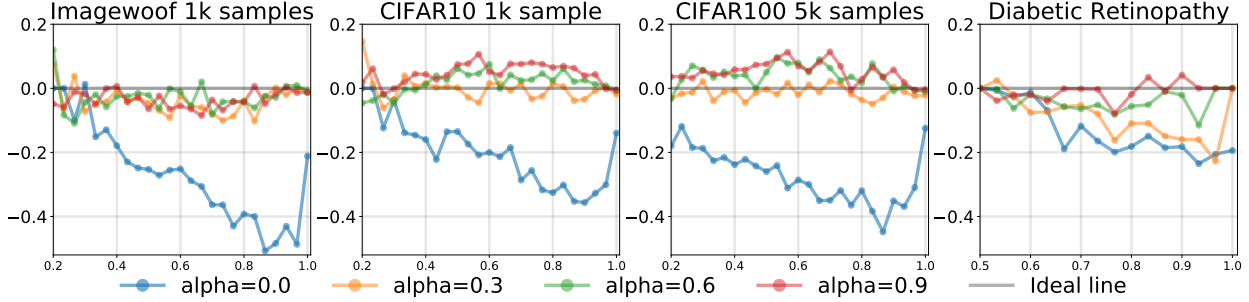


Figure 3: Calibration curve of single neural networks trained with different amount of mixup-augmentation on the IMAGEWOOF, CIFAR10, CIFAR100 and Diabetic Retinopathy [CB09] datasets. Increasing the amount of mixup augmentation consistently makes the predictions *less*-confident. The case $\alpha = 0$ corresponds to training without an mixup-augmentation, i.e. only using standard augmentation strategies.

4 Calibrating Deep Ensembles

In order to calibrate deep ensembles, several methodologies can be considered:

- (A) Do nothing and hope that the averaging process intrinsically leads to better calibration
- (B) Calibrate each individual network before aggregating all the results
- (C) Simultaneously aggregate and calibrate the probabilistic forecasts of each individual model.
- (D) Aggregate first the estimates of each individual model before eventually calibrating the pooled estimate.

Pooling methods: as recognized in the operation research literature [JW08, WGCLJ19], simple pooling/aggregation rules that do not require a large number of tuning parameters are usually preferred, especially when training data is scarce. Simple aggregation rules are usually robust, conceptually easy to understand, and straightforward to implement and optimize. The standard average and median pooling of a set $\mathbf{p}^{1:K}$ of $K \geq 2$ probabilistic predictions $\mathbf{p}^{(1)}, \dots, \mathbf{p}^{(K)} \in \Delta_C \subset \mathbb{R}^C$ are defined as

$$\mathbf{Agg}_{\text{avg}}(\mathbf{p}^{1:K}) = \frac{\mathbf{p}^1 + \dots + \mathbf{p}^K}{K} \quad \text{and} \quad \mathbf{Agg}_{\text{med}}(\mathbf{p}^{1:K}) = \frac{\text{median}(\mathbf{p}^1, \dots, \mathbf{p}^K)}{Z}, \quad (9)$$

for a normalization constant $Z > 0$, the median operation being executed component-wise over the $C \geq 2$ components. Finally, $\mathbf{trim}(z^{1:K})$, the trimmed mean [JW08] of K real numbers $z_1, \dots, z_K \in \mathbb{R}$, is obtained by first discarding the $1 \leq \kappa \leq K/2$ largest and smallest values before averaging the remaining elements. This means that $\mathbf{trim}(z^{1:K}) = [z_{\sigma(\kappa+1)} + \dots + z_{\sigma(K-\kappa-1)}]/(K-2\kappa)$ where $\sigma(\cdot)$

is a permutation such that $z_{\sigma(1)} \leq \dots \leq z_{\sigma(K)}$. The trimmed mean pooling method is consequently defined as

$$\mathbf{Agg}_{\text{trim}}(\mathbf{p}^{1:K}) = \frac{\mathbf{trim}(\mathbf{p}^1, \dots, \mathbf{p}^K)}{Z}, \quad (10)$$

for a normalization constant $Z > 0$, with the trimmed-averaging being executed component-wise.

Pool-Then-Calibrate: any of the above-mentioned aggregation procedure can be used as a pooling strategy before fitting a temperature τ_* by a minimizing proper scoring rules on a validation set. In all our experiment, we minimized the negative log-likelihood (i.e. cross-entropy). In other words, given a set $\mathbf{p}^{1:K}$ of $K \geq 2$ probabilistic forecasts, the final prediction is defined as

$$\mathbf{p}_* \equiv \text{Scale}[\mathbf{Agg}(\mathbf{p}^{1:K}), \tau_*] \quad \text{where} \quad \text{Scale}(\mathbf{p}, \tau) \equiv \sigma_{\text{SM}}(\log \mathbf{p} / \tau). \quad (11)$$

Note that the aggregation procedure can be carried out entirely independently from the fitting of the optimal temperature τ_* .

Joint Pool-and-Calibrate: there are several situations when the so-called *end-to-end* training strategy consisting in jointly optimizing several component of a composite system leads to increased performances [MKS⁺15, MPV⁺16, GWR⁺16]. In our setting, this means learning the optimal temperature τ_* concurrently with the aggregation procedure. The optimal temperature τ_* is found by minimizing a proper scoring rule $\text{Score}(\cdot)$ on a validation set $\mathcal{D}_{\text{valid}} \equiv \{x_i, y_i\}_{i=1}^{N_{\text{val}}}$,

$$\tau_* = \arg \min \left\{ \tau \mapsto \frac{1}{\mathcal{D}_{\text{valid}}} \sum_{i \in \mathcal{D}_{\text{valid}}} \text{Score}(\mathbf{p}_i^\tau, y_i) \right\}, \quad (12)$$

where $\mathbf{p}_i^\tau = \mathbf{Agg}[\text{Scale}(\mathbf{p}^{1:K}(x_i), \tau)] \in \Delta_C$ denotes the aggregated probabilistic prediction for sample x_i . In all our experiments, we have found it computationally more efficient and robust to use a simple grid search for finding the optimal temperature; we used $n = 100$ temperatures equally spaced on a logarithmic scale in between $\tau_{\min} = 10^{-2}$ and $\tau_{\max} = 10$.

Importance of the Pooling and Calibration order: Figure 4 shows calibration curves when individual models are temperature scaled separately (i.e. group [B] of methods), as well as when the models are scaled with a common temperature parameter (i.e. group [C] of methods). Furthermore, the calibration curves of the pooled model (group [B] and [C] of methods) are also displayed. More formally, the group [B] of methods obtains for each individual model $1 \leq k \leq K$ an optimal temperature $\tau_*^{(k)} > 0$ as solution of the optimization procedure

$$\tau_*^{(k)} = \arg \min \left\{ \tau \mapsto \frac{1}{\mathcal{D}_{\text{valid}}} \sum_{i \in \mathcal{D}_{\text{valid}}} \text{Score}(\text{Scale}[\mathbf{p}_i^k, \tau], y_i) \right\}$$

where $\mathbf{p}_i^k \in \Delta_C$ denotes the probabilistic output of the k^{th} model for the i^{th} example in validation dataset. The light blue calibration curves corresponds to the outputs $\text{Scale}[\mathbf{p}_i^k, \tau_*^{(k)}]$ for K different

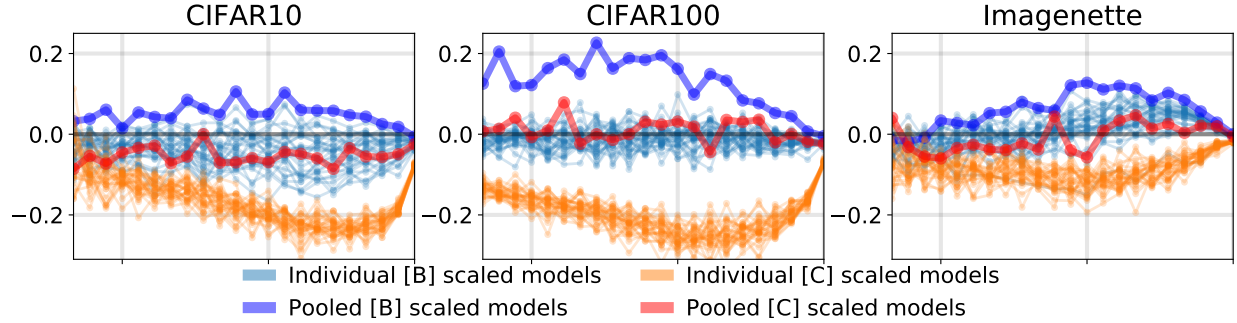


Figure 4: Calibration curve (x -axis confidence, y -axis difference between accuracy and confidence) of: **(light blue)** each model calibrated with one temperature per model (i.e. individually temperature scaled), **(dark blue)** average of individually temperature scaled models (i.e. method [B]), **(orange)** each model scaled with a global temperature obtained with method [C], **(red)** result of method [C] that consists in simultaneously aggregating and calibrating the probabilistic forecasts of each individual model. **Datasets:** a train:validation split of size 950 : 50 was used for the CIFAR10 and IMAGENETTE datasets, and of size 4700 : 300 for the CIFAR100 dataset.

models. The deep blue calibration curve corresponds the linear pooling of the individually scaled predictions. For the group [C] of methods, a single common temperature $\tau_* > 0$ is obtained as solution of the optimization procedure

$$\tau_* = \arg \min \left\{ \tau \mapsto \frac{1}{\mathcal{D}_{\text{valid}}} \sum_{i \in \mathcal{D}_{\text{valid}}} \text{Score}(\mathbf{p}_i^\tau, y_i) \right\}, \quad (13)$$

where $\mathbf{p}_i^\tau = \text{Agg}[\text{Scale}(\mathbf{p}^{1:K}(x_i), \tau)] \in \Delta_C$ denotes the aggregated probabilistic prediction for sample x_i . The orange calibration curves are generated using the predictions $\text{Scale}[\mathbf{p}_i^k, \tau_*]$ and the red one corresponds to the prediction $\text{Agg}[\text{Scale}(\mathbf{p}^{1:K}, \tau_*)]$. Notice that when scaled separately (by $\tau_*^{(k)}$) each of the individual models (light blue) is close to being calibrated, but the resulting pooled model (deep blue) is under-confident. However, when scaled by a common temperature, the optimization chooses a temperature τ_* that makes the individual models (orange) slightly over-confident, so that the resulting pooled model is nearly calibrated. This is in line with the findings discussed in section 3 and it also shows why the ordering of pooling and scaling is important.

Figure 5 compares the four methodologies **A-B-C-D** identified at the start of this section, with the three different pooling approaches Agg_{avg} and Agg_{med} and Agg_{trim} . These methods are compared to the baseline approach (in dashed red line) consisting of fitting a single network trained with the same amount $\alpha = 1$ of mixup augmentation before being temperature scaled. All the experiments are executed 50 times, on the *same* training set, but with 50 different validation sets of size $N_{\text{val}} = 50$ for CIFAR10, IMAGENETTE, IMAGEWOOF and $N_{\text{val}} = 300$ for CIFAR100, and $N_{\text{val}} = 500$ for the Diabetic Retinopathy dataset. The results indicate that on most metrics and datasets, the (naive) method **(A)** consisting of simply averaging predictions is not competitive. Secondly, and as explained in the previous section, the method **(B)** consisting in first calibrating the individual networks before pooling the predictions is less efficient across metrics than the last

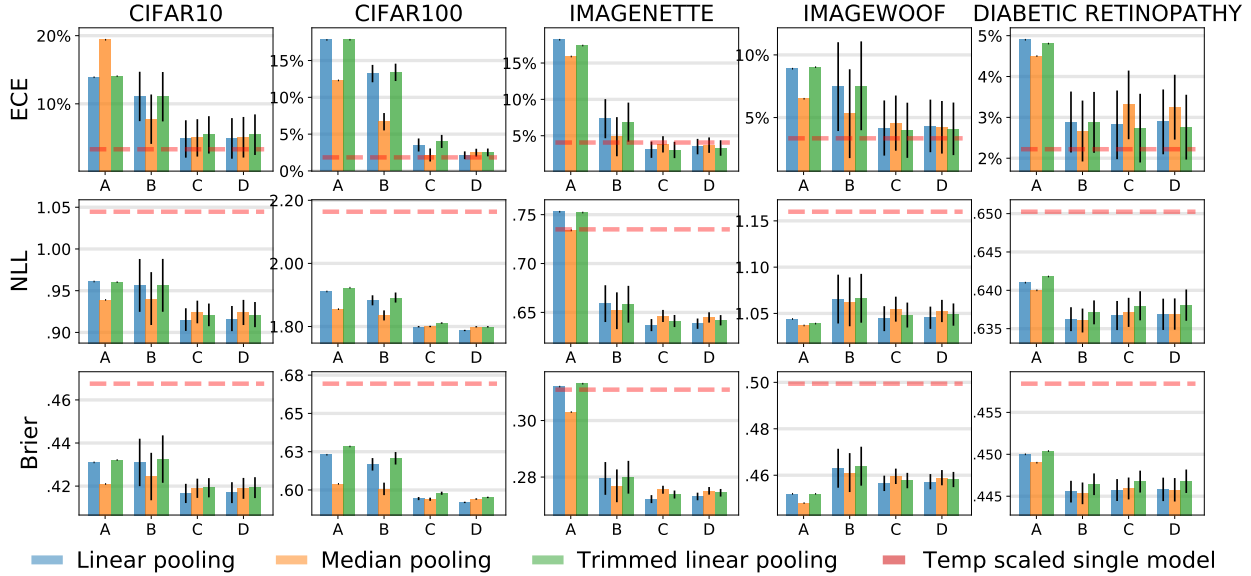


Figure 5: Performance of different pooling strategies (A–D) with $K = 30$ models trained with mixup-augmentation ($\alpha = 1$) across multiple datasets. The total datasets (training + validation) were of size $N = 1000$ for CIFAR10 and IMAGENETTE and IMAGEWOOF, and $N = 5000$ for CIFAR100 and DIABETIC RETINOPATHY. Experiments were executed 50 times on the same training data but different validation sets. The dashed red line represents a baseline performance when a single model was training with mixup augmentation ($\alpha = 1$) and post-processed with temperature scaling.

two methods (C – D). Finally, the two methods (C – D) perform comparably, the method (D) (i.e. *pool-then-calibrate*) being slightly more straightforward to implement. As regards the pooling methods, the intuitive robustness of the *median* and *trimmed-averaging* approaches does not seem to lead to any consistent gain across metrics and datasets. Note that ensembling a set of $K = 30$ networks (without any form of post-processing) does lead to a very significant improvement in NLL and Brier score but lead to a serious deterioration of the ECE. The *Pool-Then-Aggregate* methodology allows to benefit from the gains in NLL/Brier score, without compromising any loss in ECE.

Importance of the validation set: it would be practically useful to be able to fit the temperature without relying on a validation set. We report that using the training set instead (obviously) does not lead to better calibrated models (i.e. the optimal temperature is close to $\tau_* \approx 1$). We have tried to use a different amount of mixup-augmentation (and other types of augmentation) on the training set for fitting the temperature parameter, but have not been able to obtain satisfying results.

Size of the ensembles: Figure 7 shows the performance of the different pooling methods (i.e. groups [B]–[D]) on the CIFAR10 dataset, as a function of the number of individual models in the ensemble. For clarity, the (non-calibrated) group [A] of methods are not reported. Recall that the group [A] pools the the predictions without any calibration procedure, the group [B] first calibrates each individual models separately before aggregating the results, the group [C] jointly calibrates and aggregates the prediction, and finally the group [D] first aggregates the results

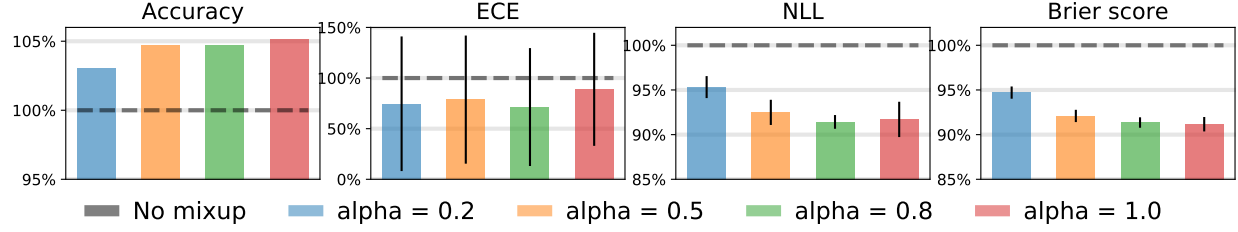


Figure 6: *Pool-Then-Calibrate* approach when applied to a deep-ensemble of $K = 30$ networks trained with different amount of mixup-augmentation on $N = 1000$ CIFAR10 training samples (out of which $N_{\text{val}} = 50$ were used for validation). For each metric, we report the **ratio** of performance when compared to the *Pool-then-Calibrate* method used without any form of mixup-augmentation (but with standard data-augmentation). The results indicate a clear benefit in using the mixup-augmentation in conjunction to temperature scaling. Experiments were executed on 50 different validation sets (the errorbars show the variation), and a fixed training set of 950 samples.

before calibrating the resulting prediction. Methods in group [C] and [D] performs similarly. For the CIFAR10 dataset, we observe that the performance under most metrics saturates for ensemble of sizes ≈ 15 .

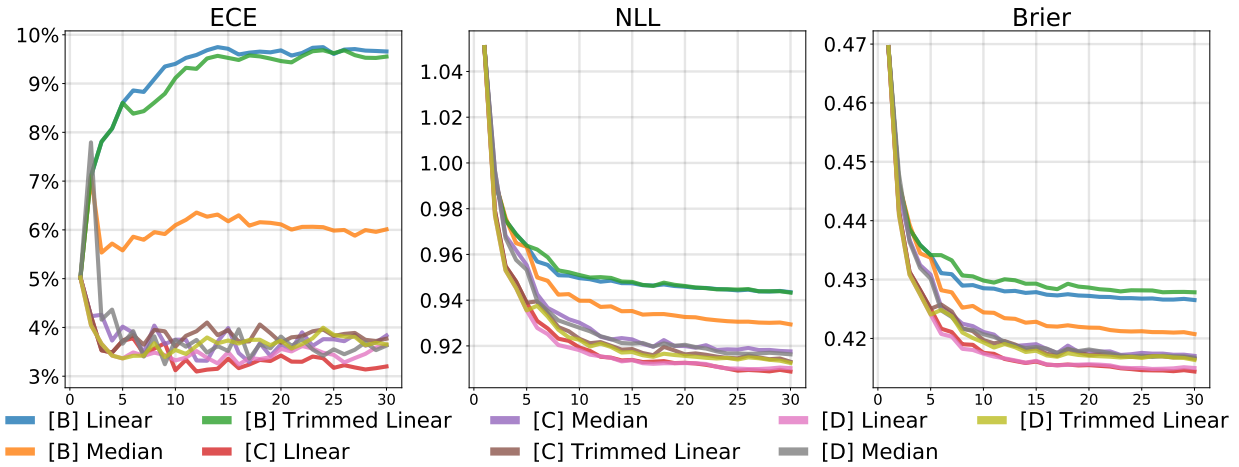


Figure 7: Comparison of methods **B-C-D** described at the start of Section 4 on the CIFAR10 dataset with $N = 1000$ samples (950:50 split). The x -axis denotes the number of models. To avoid clutter and due to significantly worse performance, method **[A]** (i.e. standard deep-ensemble without any form of calibration) is omitted.

Table 1 reports the numerical results obtained when a linear averaging aggregation method is used within each group **[A]**–**[D]** of calibration procedures. Experiments are carried-out on 50 different validation sets (and a single training set).

Role and effect of mixup-augmentation: the mixup augmentation strategy is popular and straightforward to implement. As already empirically described in Section 3, increasing the amount of mixup-augmentation typically leads to a decrease in the confidence and increase in entropy of the predictions. This can be beneficial in some situations but also indicates that this approach should certainly be employed with care for producing calibrated probabilistic predictions. Contrarily to other geometric data-augmentation transformations such as image flipping,

rotations, and dilatations, the mixup strategy produces non-realistic images that consequently lie outside the data-manifold of natural images: this typically leads to a large distributional shift. The mixup strategy relies on a subtle trade-off between the increase in training data diversity, which can help mitigate over-fitting problems, and the distributional shift that can be detrimental to the calibration properties of the resulting method. Figure 6 compares the performance of the *Pool-Then-Calibrate* approach when applied to a deep-ensemble of $K = 30$ networks trained with different amount of mixup-augmentation. The results are compared to the same approach (i.e. *Pool-then-Calibrate* with $K = 30$ networks) with no mixup-augmentation. The results indicate a clear benefit in using the mixup-augmentation in conjunction with temperature scaling.

Ablation study: For our ablation study, we focus on the CIFAR10 dataset with 1000 examples. As mentioned earlier, we reduce the training dataset by 50 training examples for steps involving the validation dataset. Similar to table 1 we evaluate methods requiring post-processing optimization on a random set of 50 different validation datasets. We provide the results of our ablation study in table 2. For setups involving training a single model, we report mean and standard deviations of the metric from a variety of 30 different trained models.

Cold posteriors: the article [WRV⁺20] reports gains in several metrics when fitting Bayesian neural networks to a *tempered posterior* of type $\pi_\tau(\theta) \propto \pi(\theta)^{1/\tau}$, where $\pi(\theta)$ is the standard Bayesian posterior, for temperatures τ *smaller than one*. Although not identical to our setting, it should be noted that in all our experiments, the optimal temperature τ_* was consistently smaller than one. In our setting, this is because simply averaging predictions lead to under-confident results. We postulate that related mechanisms are responsible for the observations reported in [WRV⁺20].

5 Discussion

The problem of calibrating deep-ensembles has received surprisingly little attention in the literature. In this text, we examined the interaction between three of the most simple and widely used methods for scaling deep-learning to the low-data regime: ensembling, temperature scaling, and mixup data-augmentation. We highlight that ensembling in itself does not lead to better-calibrated predictions, that the mixup augmentation strategy is practically important and relies on non-trivial trade-offs, and that these methods subtly interact with each other. Crucially, we demonstrate that the order in which the pooling and temperature scaling procedures are executed is important to obtaining calibrated deep-ensembles. We advocate the *Pool-Then-Calibrate* approach consisting of first pooling the individual neural network predictions together before eventually post-processing the result with a simple and robust temperature scaling step. Furthermore, we note that this approach is insensitive to the choice of pooling method, the simple linear averaging procedure being essentially as robust as the *median* and *trimmed averaging* methods.

CIFAR10 1000 samples

Metric	Group [A] Linear Pool	Group [B] Linear Pool	Group [C] Linear Pool	Group [D] Linear Pool
test acc	70.67	69.94	69.93	69.95
test ECE	13.9	11.1 \pm 3.6	4.8 \pm 2.7	4.9 \pm 2.9
test NLL	0.961	0.956 \pm .031	0.915 \pm .013	0.916 \pm .015
test BRIER	0.431	0.431 \pm .011	0.416 \pm .004	0.417 \pm .005

CIFAR100 5000 samples

test acc	55.32	54.03	53.99	54.05
test ECE	17.8	13.1 \pm 1.2	3.5 \pm 0.9	2.1 \pm .5
test NLL	1.911	1.883 \pm .016	1.799 \pm .002	1.787 \pm .002
test BRIER	0.623	0.616 \pm 0.004	0.594 \pm .001	0.592 \pm .0

Diabetic Retinopathy 5000 samples

test acc	64.38	64.41	64.34	64.38
test ECE	4.9	2.8 \pm .7	2.8 \pm .8	2.9 \pm .8
test NLL	0.641	0.636 \pm .001	0.637 \pm .002	0.637 \pm .002
test BRIER	0.450	0.445 \pm .001	0.445 \pm .001	0.446 \pm .001

Imagewoof 1000 samples

test acc	66.89	66.05	66.05	66.03
test ECE	8.9	7.5 \pm 3.5	4.2 \pm 2.2	4.3 \pm 2.1
test NLL	1.044	1.065 \pm 0.26	1.044 \pm .013	1.045 \pm 0.12
test BRIER	0.452	0.463 \pm .008	0.456 \pm .003	0.457 \pm .003

Imagenette 1000 samples

test acc	80.91	80.72	80.74	80.75
test ECE	18.2	7.3 \pm 2.7	3.1 \pm 1.1	3.5 \pm 1.0
test NLL	0.753	0.659 \pm .018	0.637 \pm .006	0.638 \pm .005
test BRIER	0.312	0.279 \pm .005	0.272 \pm .001	0.273 \pm .001

Table 1: Numerical table for the performance of linear pooling under different groups ([A]-[D]) and different datasets. The number of samples used for different setup are the same as mentioned in the main text. The mean and standard deviation is reported out of 50 different validation sets.

Metric	(Ours) 30 models temp scaled Augment + mixup	30 models mixup Augment	single model mixup Augment	single model no mixup Augment	single model no mixup no Augment
test acc	69.92 \pm .04	70.67	66.45 \pm .61	63.73 \pm .51	49.85 \pm .66
test ECE	3.3 \pm 1.9	13.9	7.03 \pm .7	20.7 \pm .4	23.4 \pm 1.0
test NLL	0.910 \pm .012	0.961	1.03 \pm .13	1.509 \pm .017	1.770 \pm .045
test BRIER	0.414 \pm .002	0.431	0.463 \pm .005	0.556 \pm .006	0.718 \pm .009

Table 2: Ablation study performed on CIFAR10 1000 samples. For ensemble temp scaling we use 950 training samples and 50 validation set. For setups with variation we report metric mean and standard deviation.

References

- [BC17] Hamed Bonab and Fazli Can. Less is more: a comprehensive framework for the number of components of ensemble classifiers. *arXiv preprint arXiv:1709.02925*, 2017.
- [BCKW15] C. Blundell, J. Cornebise, K. Kavukcuoglu, and D. Wierstra. Weight uncertainty in neural networks. *ICML*, 2015.
- [BM19] Alberto Bietti and Julien Mairal. On the inductive bias of neural tangent kernels. In *Advances in Neural Information Processing Systems*, pages 12873–12884, 2019.
- [Bri50] Glenn W Brier. Verification of forecasts expressed in terms of probability. *Monthly weather review*, 78(1):1–3, 1950.
- [CB09] Jorge Cuadros and George Bresnick. EyePACS: An Adaptable Telemedicine System for Diabetic Retinopathy Screening. *Journal of Diabetes Science and Technology*, 3(3):509–516, May 2009.
- [CKNH20] Ting Chen, Simon Kornblith, Mohammad Norouzi, and Geoffrey Hinton. A simple framework for contrastive learning of visual representations. *arXiv preprint arXiv:2002.05709*, 2020.
- [DR17] Gintare Karolina Dziugaite and Daniel M Roy. Computing nonvacuous generalization bounds for deep (stochastic) neural networks with many more parameters than training data. *arXiv preprint arXiv:1703.11008*, 2017.
- [FHL19] Stanislav Fort, Huiyi Hu, and Balaji Lakshminarayanan. Deep ensembles: A loss landscape perspective. *arXiv preprint arXiv:1912.02757*, 2019.
- [GG16] Yarin Gal and Zoubin Ghahramani. Dropout as a bayesian approximation: Representing model uncertainty in deep learning. In *international conference on machine learning*, pages 1050–1059, 2016.
- [GML⁺18] Marylou Gabrié, Andre Manoel, Clément Luneau, Nicolas Macris, Florent Krzakala, Lenka Zdeborová, et al. Entropy and mutual information in models of deep neural networks. In *Advances in Neural Information Processing Systems*, pages 1821–1831, 2018.
- [GPSW17] C. Guo, G. Pleiss, Y. Sun, and K. Q. Weinberger. On calibration of modern neural networks. *Proceedings of the 34 th International Conference on Machine Learning, Sydney, Australia, PMLR 70*, 2017, 2017.
- [GR07] Tilmann Gneiting and Adrian E Raftery. Strictly proper scoring rules, prediction, and estimation. *Journal of the American statistical Association*, 102(477):359–378, 2007.
- [Gra11] A. Graves. Practical variational inference for neural networks. *NIPS*, 2011.

- [GWR⁺16] Alex Graves, Greg Wayne, Malcolm Reynolds, Tim Harley, Ivo Danihelka, Agnieszka Grabska-Barwińska, Sergio Gómez Colmenarejo, Edward Grefenstette, Tiago Ramalho, John Agapiou, et al. Hybrid computing using a neural network with dynamic external memory. *Nature*, 538(7626):471–476, 2016.
- [HFW⁺19] Kaiming He, Haoqi Fan, Yuxin Wu, Saining Xie, and Ross Girshick. Momentum contrast for unsupervised visual representation learning. *arXiv preprint arXiv:1911.05722*, 2019.
- [How] Jeremy Howard. Imagenette and imagewoof.
- [JGH18] Arthur Jacot, Franck Gabriel, and Clément Hongler. Neural tangent kernel: Convergence and generalization in neural networks. In *Advances in neural information processing systems*, pages 8571–8580, 2018.
- [JW08] Victor Richmond R Jose and Robert L Winkler. Simple robust averages of forecasts: Some empirical results. *International journal of forecasting*, 24(1):163–169, 2008.
- [LPB17] B. Lakshminarayanan, A. Pritzel, and C. Blundell. Simple and scalable predictive uncertainty estimation using deep ensembles. *31st Conference on Neural Information Processing Systems, Long Beach, CA, USA*, 2017.
- [LPC⁺15] Stefan Lee, Senthil Purushwalkam, Michael Cogswell, David Crandall, and Dhruv Batra. Why m heads are better than one: Training a diverse ensemble of deep networks. *arXiv preprint arXiv:1511.06314*, 2015.
- [LW16] C. Louizos and M. Welling. Structured and efficient variational deep learning with matrix gaussian posteriors. *arXiv preprint arXiv:1603.04733*, 2016.
- [Mac92] D. J. C. MacKay. A practical bayesian framework for backpropagation networks. *Neural Computation*, 4(3):448–472, 1992.
- [MGI⁺19] W. Maddox, T. Garipov, P. Izmailov, D. Vetrov, and A. G. Wilson. A simple baseline for bayesian uncertainty in deep learning. *arXiv preprint arXiv:1902.02476*, 2019.
- [MKS⁺15] Volodymyr Mnih, Koray Kavukcuoglu, David Silver, Andrei A Rusu, Joel Veness, Marc G Bellemare, Alex Graves, Martin Riedmiller, Andreas K Fidjeland, Georg Ostrovski, et al. Human-level control through deep reinforcement learning. *Nature*, 518(7540):529–533, 2015.
- [MMK03] David JC MacKay and David JC Mac Kay. *Information theory, inference and learning algorithms*. Cambridge university press, 2003.
- [MMN18] Song Mei, Andrea Montanari, and Phan-Minh Nguyen. A mean field view of the landscape of two-layer neural networks. *Proceedings of the National Academy of Sciences*, 115(33):E7665–E7671, 2018.

- [MPV⁺16] Piotr Mirowski, Razvan Pascanu, Fabio Viola, Hubert Soyer, Andrew J Ballard, Andrea Banino, Misha Denil, Ross Goroshin, Laurent Sifre, Koray Kavukcuoglu, et al. Learning to navigate in complex environments. *arXiv preprint arXiv:1611.03673*, 2016.
- [Nea12] Radford M Neal. *Bayesian learning for neural networks*, volume 118. Springer Science & Business Media, 2012.
- [Pla99] J. Platt. Probabilistic outputs for support vector machines and comparisons to regularized likelihood methods. *Advances in Large Margin Classifiers*, 10(3), 1999.
- [Pre98] Lutz Prechelt. Early stopping-but when? In *Neural Networks: Tricks of the trade*, pages 55–69. Springer, 1998.
- [PW17] Luis Perez and Jason Wang. The effectiveness of data augmentation in image classification using deep learning. *arXiv preprint arXiv:1712.04621*, 2017.
- [RMW14] Danilo Jimenez Rezende, Shakir Mohamed, and Daan Wierstra. Stochastic backpropagation and approximate inference in deep generative models. *arXiv preprint arXiv:1401.4082*, 2014.
- [RVE18] Grant M Rotskoff and Eric Vanden-Eijnden. Neural networks as interacting particle systems: Asymptotic convexity of the loss landscape and universal scaling of the approximation error. *arXiv preprint arXiv:1805.00915*, 2018.
- [SHK⁺14] Nitish Srivastava, Geoffrey Hinton, Alex Krizhevsky, Ilya Sutskever, and Ruslan Salakhutdinov. Dropout: a simple way to prevent neural networks from overfitting. *The Journal of Machine Learning Research*, 15(1):1929–1958, 2014.
- [SLJ⁺15] Christian Szegedy, Wei Liu, Yangqing Jia, Pierre Sermanet, Scott Reed, Dragomir Anguelov, Dumitru Erhan, Vincent Vanhoucke, and Andrew Rabinovich. Going deeper with convolutions. In *Proceedings of the IEEE conference on computer vision and pattern recognition*, pages 1–9, 2015.
- [WGCLJ19] Robert L. Winkler, Yael Grushka-Cockayne, Kenneth C. Lichtendahl, and Victor Richmond R. Jose. Probability forecasts and their combination: A research perspective. *Decision Analysis*, 16(4):239–260, 2019.
- [WHSX16] Andrew G Wilson, Zhiting Hu, Ruslan R Salakhutdinov, and Eric P Xing. Stochastic variational deep kernel learning. In *Advances in Neural Information Processing Systems*, pages 2586–2594, 2016.
- [WI20] Andrew Gordon Wilson and Pavel Izmailov. Bayesian deep learning and a probabilistic perspective of generalization. *arXiv preprint arXiv:2002.08791*, 2020.
- [WRV⁺20] Florian Wenzel, Kevin Roth, Bastiaan S Veeling, Jakub Świątkowski, Linh Tran, Stephan Mandt, Jasper Snoek, Tim Salimans, Rodolphe Jenatton, and Sebastian Nowozin. How good is the bayes posterior in deep neural networks really? *arXiv preprint arXiv:2002.02405*, 2020.

- [YZYC19] Mang Ye, Xu Zhang, Pong C Yuen, and Shih-Fu Chang. Unsupervised embedding learning via invariant and spreading instance feature. In *Proceedings of the IEEE Conference on Computer Vision and Pattern Recognition*, pages 6210–6219, 2019.
- [ZBH⁺16] Chiyuan Zhang, Samy Bengio, Moritz Hardt, Benjamin Recht, and Oriol Vinyals. Understanding deep learning requires rethinking generalization. *arXiv preprint arXiv:1611.03530*, 2016.
- [ZCDL17] Hongyi Zhang, Moustapha Cissé, Yann N. Dauphin, and David Lopez-Paz. mixup: Beyond empirical risk minimization. *CoRR*, abs/1710.09412, 2017.
- [ZH05] Hui Zou and Trevor Hastie. Regularization and variable selection via the elastic net. *Journal of the royal statistical society: series B (statistical methodology)*, 67(2):301–320, 2005.